

## STUDY OF THE MICROSTRUCTURE OF HIGH REFLECTIVITY FILMS ON CERAMIC GLAZES

F. Sanmiguela<sup>(1)</sup>, O. Ruiza<sup>(1)</sup>, S. Sorlib<sup>(2)</sup>, G. Monrósb<sup>(2)</sup>

<sup>(1)</sup>TORRECID S.A., Alcora (Spain), <sup>(2)</sup>Dept. of Inorganic and Organic Chemistry, Universidad Jaume I, Castellón (Spain).

### ABSTRACT

*The present paper sets out the study undertaken of the microstructure of films of lustres based on different oxides, on ceramic glazes. The deposited layers have been characterized by X-ray diffraction with a low angle of incidence, diffuse reflectance UV-V spectroscopy, scanning electron microscopy, energy-dispersive X-ray microanalysis (EDX), differential interferometry and atomic force microscopy. The results show the precipitation in firing of nanostructured layers of 4-14 nm size nanocrystals, which form 40-150 nm aggregates. The high refractive index and low roughness of the deposited layer determine the high reflectivity for generating the lustre effect. The size of the aggregates determines surface roughness, while it is necessary to avoid high aggregation in order to maintain the high gloss that characterizes these materials.*

## 1. INTRODUCTION

The reflectivity  $R$  of a material is defined as the fraction of light reflected at the material-air interface and is related to the refractive index by means of the Fresnel equation:

$$R = \left( \frac{n-1}{n+1} \right)^2 \quad (\text{eq. 1})$$

where  $n$  is the refractive index. The value of this index is around 1.5 for silica glasses, whereas for glasses opacified with zirconium silicate this rises to 1.6-1.7. The transition metal oxides, like  $\text{Fe}_2\text{O}_3$  or  $\text{Co}_3\text{O}_4$ , display refractive indices of 1.7-1.9, reaching up to 2.7 in the case of anatase ( $\text{TiO}_2$ ), which is therefore a highly refringent medium <sup>[1]</sup>.

On the other hand, the reflection of light at an interface between two media with a different refractive index presents a different scattering depending on the angle of incidence  $\theta$  between the directions of the incident beams and the direction normal to the surface. Gloss in the direction  $\theta$  (expressed by the angle formed with the normal to the interface) can be defined from the relation:

$$B = \frac{I_\theta}{A_\theta} \quad (\text{eq. 2})$$

where  $B$  is gloss,  $I_0$  is the reflected intensity and  $A_0$  the normal elementary area, all in the direction  $\theta$ .

Reflection is termed diffuse reflection when the light scatter at the surface obeys the law of cosine:

where  $I_0$  is the intensity dispersed at  $\theta=0$ . Thus, gloss in a given direction  $\theta$  is constant:

$$I_\theta = I_0 \cos\theta \quad (\text{eq. 3})$$

If the scatter is zero in all directions except in the reflected direction  $\theta=i$ , where  $i$  is the angle of incidence of the light beam, the reflection is specular.

$$B = \frac{I_0 \cos\theta}{A_0 \cos\theta} = \frac{I_0}{A_0} = \text{constante} \quad (\text{eq. 4})$$

Thus, specular reflection is related to extremely smooth surfaces, whereas diffuse reflection is related to rough surfaces.

The resulting gloss of a surface is mainly the result of the conjunction of these two factors: the refractive index of the material (high reflectivity) and the roughness of the surface. Therefore, if the thermal deposition of fine metallic oxide layers with a high refractive index and low roughness can be achieved, they may be expected to display high gloss effects <sup>[2]</sup>.

Now in the field of third-fire ceramics, highly reflective coatings are being produced from screen printing inks containing metallic cations, which have been incorporated as thermally unstable metallic salts or alkoxides, such as nitrates or chlorides<sup>[3]</sup>. The present study has specifically addressed the formation of highly reflective films from precursors of Ti, Fe and Co on glazes of molar composition  $0.2\text{CaO}\cdot 0.15\text{ZnO}\cdot 0.05\text{K}_2\text{O}\cdot 0.1\text{Al}_2\text{O}_3\cdot 0.45\text{SiO}_2\cdot 0.05\text{ZrO}_2$ , which crystallize zircon in small quantities. These films have been examined from a microstructural point of view to ascertain the origin of the high resulting gloss. The influence of parameters such as precursor concentration, or heat-treatment temperature and time, has also been evaluated.

## 2. EXPERIMENTAL

The preparation of the inks was carried out by adding the necessary quantity of corresponding precursor (Ti, Fe or Co), to a certain amount of hydroalcoholic solvent and screen printing vehicle, and subjecting the mixture to stirring until obtaining thorough homogenization of the precursor in the vehicle. In the case of Fe and Co, the corresponding nitrates, nonahydrate and hexahydrate respectively, were used as precursors, whereas in the case of Ti, t-butoxide was used. A mixture of alcohols and thickeners of the cellulose type were used as screen printing vehicles, so that the resulting screen printing pastes displayed the appropriate conditions for application by screen printing on previously fired glazes. A porous glaze of molar composition  $0.2\text{CaO}\cdot 0.15\text{ZnO}\cdot 0.05\text{K}_2\text{O}\cdot 0.1\text{Al}_2\text{O}_3\cdot 0.45\text{SiO}_2\cdot 0.05\text{ZrO}_2$  with a tendency to crystallize zircon in small quantities was used. After application of the screen printings, the samples were subjected to the corresponding heat treatment of the study involved.

The materials used were characterized by differential thermal analysis with a Perkin Elmer differential calorimeter at a heating rate of  $10^\circ\text{C}/\text{min}$ , using  $\alpha\text{-Al}_2\text{O}_3$  as a standard. In order for the signal corresponding to the precursor not to be completely overlapped by the signal of the screen printing vehicle, this study was conducted using a 9% cation content. The glaze was characterized by hot stage microscopy to determine the characteristic sintering, softening, half-sphere and 1/3 sphere points.

The study of the resultant high reflectivity layers was carried out with the following techniques:

a) Grazing incidence X-ray diffraction or with a low angle of incidence: this technique is necessary given the limitation that conventional diffractometers display in studying fine layers, as the penetration of X-rays in the sample is much greater than the thickness of the layer being studied, causing detection of underlying crystals. When a non-modified powder diffractometer is used, the distance travelled through the layer is short and the peaks obtained are too wide and diffuse. In contrast, when the surface of the sample is exposed to low angle radiation (typically  $2\theta \leq 2^\circ$ ), the effective length of the beam crossing the surface increases an order of magnitude. In the surface incidence device the conventional Bragg-Brentano X-ray focalization is converted into a decoupled parallel beam<sup>[4]</sup>, for which it is necessary to mount an accessory with long Soller slits with sheets perpendicular to the diffraction plane. In this study, performed in a Siemens D5000 diffractometer, we used a low divergence slit,  $0.1^\circ$ , a Soller slit to limit the axial divergence on the side of the tube and long slits on the side of the detector (divergences of 0.2 or 0.4)

b) UV-V-NIR spectroscopy: a Perkin Elmer Lambda 2000 spectrophotometer was used, working by the diffuse reflectance method. The spectra of semiconducting

materials such as the ones studied exhibit a charge transfer band in the UV-V frequency range that moves to shorter wavelengths (higher energies) when the particle size of the material is nanometric. The energy of the semiconductor band gap, which is required for conductivity, is measured from the spectrum absorption frequency threshold. In accordance with the above, the band gap energy of the nanometric material  $E$  is greater than that of the monolithic material  $E_g$ , in which the difference is inversely proportional to the particle radius in accordance with Eq. 5 and in accordance with the theoretical studies <sup>[5],[6]</sup>:

$$E = E_g + \frac{h^2\pi^2}{8\mu R^2} \quad (\text{eq. 5})$$

where  $E_g$  is the band gap for the semiconductor,  $h$  is the Planck constant and  $\mu$  is the reduced mass of the electron-vacant pair ( $\approx 0.08m_0$ ,  $m_0$  = mass of the proton at rest).

c) CIEL\*a\*b\* colorimetry associated with the Perkin Elmer Lambda 2000 UV-V-NIR spectrophotometer. In this colorimetric methodology, parameter L measures the intensity or lightness of the colour (from 0 for white to 100 for black),  $a^*$  measures the evolution green ( $a^* < 0$ ) to red ( $a^* > 0$ ) and parameter  $b^*$  the variation of blue ( $b^* < 0$ ) to yellow ( $b^* > 0$ ) <sup>[7]</sup>.

d) SEM-EDX (scanning electron microscopy coupled with X-ray energy dispersion analysis): this technique enabled analyzing the surface of the deposited material and its chemical composition.

e) The gloss of the deposited layers was measured by a Minolta 268 glossmeter using the conventional method of photometric comparison with a standard glass at different angles of incidence.

f) To measure the degree of roughness of the surface, the conventional method was used by a pick-up on a Kosaka Laboratory Ltd. SM-3 roughness meter. This method provides the mean of the deviations in respect of the base line  $R_a$  (mean roughness) in a travel of around 5-10 cm of the pick-up on the surface. Using the differential interferometry method, the micrometric roughness was analyzed by optical reflection measurements of the same beam on the test surface and a standard surface. The difference between both reflections is proportional to the local topography of the incision zone (of the order of 0.1x0.1 mm). Finally, the local roughness of the surface, analyzed on a nanometric scale, was evaluated by AFM (atomic force microscopy).

### 3. RESULTS AND DISCUSSION

#### 3.1. GLAZED SURFACE AND SCREEN PRINTING INK INTERACTION MODEL

Figure 1 depicts the differential thermal analysis of the three inks used, which each contain 9% of the corresponding cation (Fe, Ti or Co) with a view to enable detecting the crystallization bands.

Thermal analysis of the inks indicates a set of endothermic bands, which are broad and not very intense at low temperature, associated with the evaporation of the

organic components: doublet for Fe at 100 and 125°C, broad and not very intense band centred at 140°C for Co, and weak and broad band at 160°C for Ti (Figure 1). Subsequently, carbonization and combustion of the organic materials occurs: for Fe the combustion band centres at 175°C, for Co two very sharp bands appear located at 175 and 250°C, and for Ti the band begins at 230°C and displays a sharp maximum at 275°C. Finally, differential thermal analysis of the inks show the oxide crystallization bands, which are very clear for Ti with two broad and intense bands at 410 and 510°C, for Co a not very intense band at 280°C up against the combustion band, and for Fe an intense band at 275°C, which mixes with the combustion band.

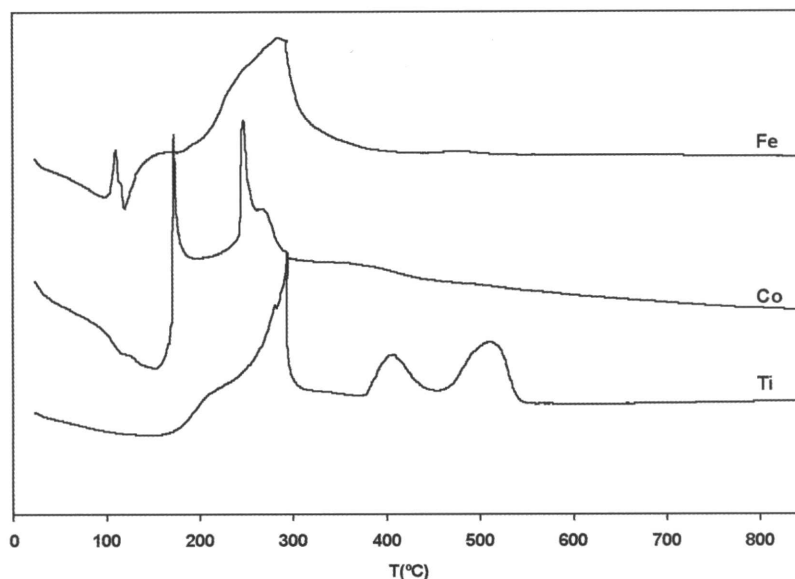


Figure 1. Differential thermal analysis of the three inks used, with 9% cation (Fe, Co or Ti) content.

The glaze used was a porous single-fire glossy glaze based on the system ZnO-CaO-SiO<sub>2</sub>-ZrO<sub>2</sub> with a tendency to devitrify zircon in small quantities. Hot stage microscopy analysis of this glaze indicates a sintering temperature around 900°C, softening temperature at 1040°C, half-sphere at 1150°C and 1/3 sphere at 1200°C.

Based on these data, a fired glazed surface and screen printing ink interaction model can be proposed, which contemplates the following stages <sup>[8], [9]</sup>:

- a) Uniform ink deposition on the glaze owing to the low surface tension of the glaze and high viscosity of the vehicle.
- b) Independent thermal evolution of the ink up to the glaze sintering temperature (900°C): combustion occurs of the organic materials in the vehicles around 150-250°C, the carbonized material is liquid since the melting points of the precursor used are low, and this is followed by decomposition of the fused salt (nitrate or alkoxide) around 300-400°C. The oxide generated in the decomposition crystallizes by heterogeneous nucleation due to the nucleating effect of the glaze surface, which allows uniform crystallization over the entire surface, producing a film of nanocrystals that form aggregates at each arising nucleation point. The viscosity of the glaze has decreased sufficiently to allow glaze-film interaction and generation of a bonding interface. Were this not the case, the film would not interact with the glaze and would readily detach on cooling.

c) Thermal evolution of the nanocrystalline film starting from the sintering temperature: above this temperature, glaze viscosity decreases rapidly, which causes the glaze to begin solubilizing the oxide formed. On the other hand, the oxide increases its vapour pressure and the film progressively vanishes by evaporation. In addition, coarsening occurs by thermal maturing of the particles in the aggregates. In this stage, film thickness decreases at a growing rate, by a combined effect of volatilization when temperature increases and solubilization when glaze viscosity decreases. In general, almost complete loss of the film can be expected around the glaze softening temperature.

### 3.2. SCREEN PRINTING DEPOSITION OF FILMS FROM IRON, COBALT AND TITANIUM PRECURSORS.

Table 1 sets out the results obtained with the different techniques used for films deposited with inks that contained 0.6% by weight of the metal, heat treated at 820°C for 5 minutes.

Sample	Gloss (85°)	Colorimetry (L*/a*/b*)	XRD	Roughness R <sub>a</sub>		Nanocrystal radius	Agglomerates (AFM)
				Pick-up	Interferometry		
Glaze	96	99/0/0	Zircon	0.05 μm	18 nm	--	--
Fe film	100	84/11/21	Zircon Hematita	0.05 μm	40 nm	5.2 nm	75 nm
Co film	97	72/-2/11	Zircon Co <sub>3</sub> O <sub>4</sub>	0.05 μm	34 nm	11.3 nm	75 nm
Ti film	103	97/-1/2	Zircon Anatase	0.05 μm	21 nm	14.0 nm	40 nm

Table 1: Results corresponding to the glaze and films with 0.6% cation heat treated at 820°C for 5 min. Gloss, colorimetry, grazing incidence XRD, millimetric and micrometric roughness, nanocrystal radius according to Eq. 5 and size of the agglomerates measured by AFM.

The results of surface incidence XRD (Figure 2.a) indicate the presence of H (hematite Fe<sub>2</sub>O<sub>3</sub>), C (cobalt spinel Co<sub>3</sub>O<sub>4</sub>) and A (TiO<sub>2</sub> anatase), next to peaks of Z (ZrSiO<sub>4</sub> zircon) devitrified in the glaze. The peak intensities of the crystalline phases in the films are 1/5 that of the underlying devitrified zircon, and they are not detected with a conventional diffraction configuration, indicating that the films are extremely thin. In fact, scanning electron microscopy, SEM, with backscattered electron detector in normal operation does not allow observing the crystallization detected by XRD, either in a surface or cross-sectional view, only observing the acicular zircon devitrified by the glaze (Figure 2.b), although it is possible to detect the presence of the oxide cation by means of X-ray energy dispersion analysis (EDX) (Figure 2.c).

The values of CIEL\*a\*b\* colorimetry in Table 1 indicate the generation of a red-yellow colour layer of average intensity (L\*a\*b\*=84/11/21) in the case of hematite, a dark greenish yellow colour (L\*a\*b\*=72/-2/11) for the cobalt spinel, and a metallized grey colour for anatase (L\*a\*b\*=97/-1/2).

The gloss values measured by means of the glossmeter with an angle of incidence of 85°, by comparison with the standard surface to which a value of 100 was

given, indicate that the base is a glossy glaze (B=96) and that the spinel film  $\text{Co}_3\text{O}_4$  displays a similar or slightly superior gloss (B=97), while the hematite and particularly the anatase films exhibit greater reflectivity. This result is consistent with the reflectivity of the films (Eq. 1), since the glaze with zircon has a refractive index of 1.6 and the compounds  $\text{Co}_3\text{O}_4$ ,  $\text{Fe}_2\text{O}_3$  and  $\text{TiO}_2$  (anatase) have refractive indices of 1.7, 1.8 and 2.6 respectively. The greater refractive index of anatase explains the better development of the lustre in the film with titanium.

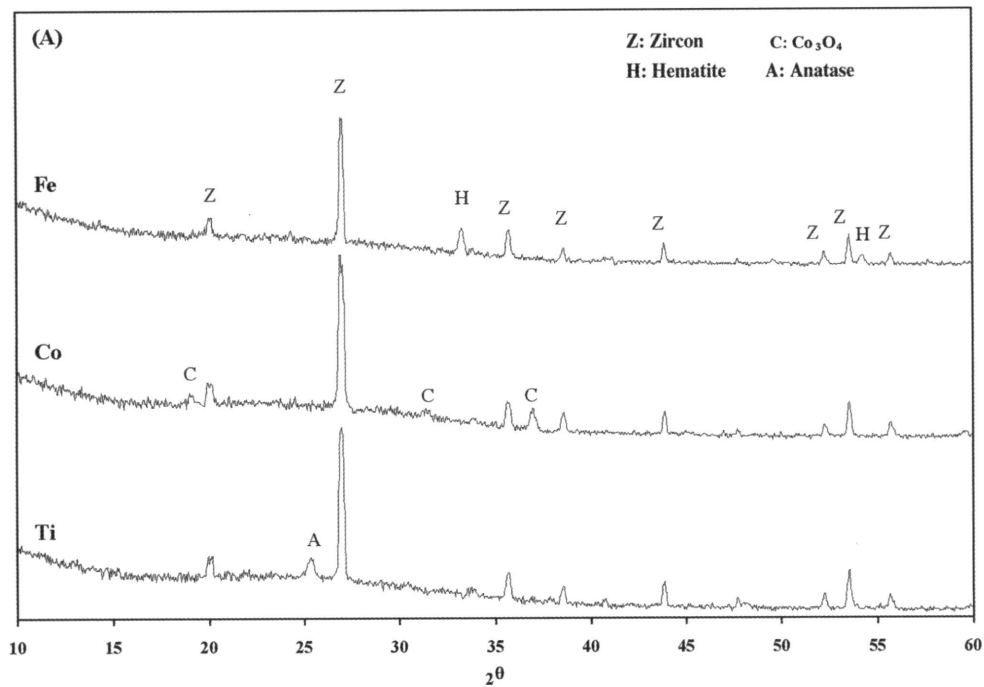


Figure 2. (A): Grazing incidence X-ray diffractograms of the Fe, Co and Ti films. Results obtained with samples with 0.6% cation content, heat treated at 820°C for 5 min.

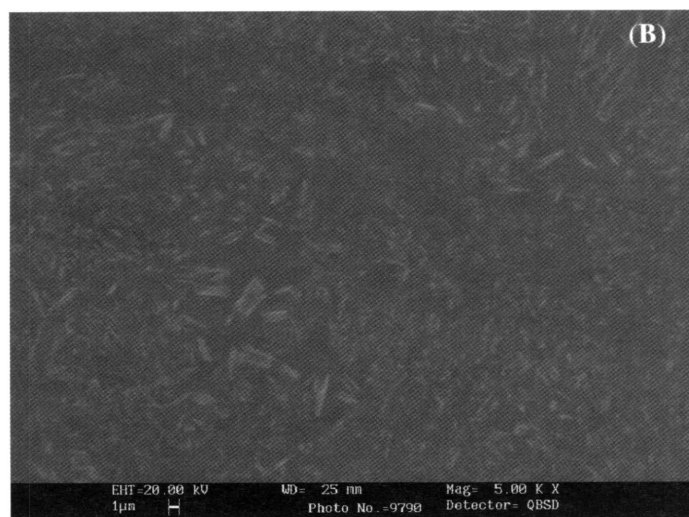


Figure 2. (B): Face SEM micrograph of the Fe sample, in which only zircon crystals are observed. Results obtained with samples with 0.6% cation content, heat treated at 820°C for 5 min.

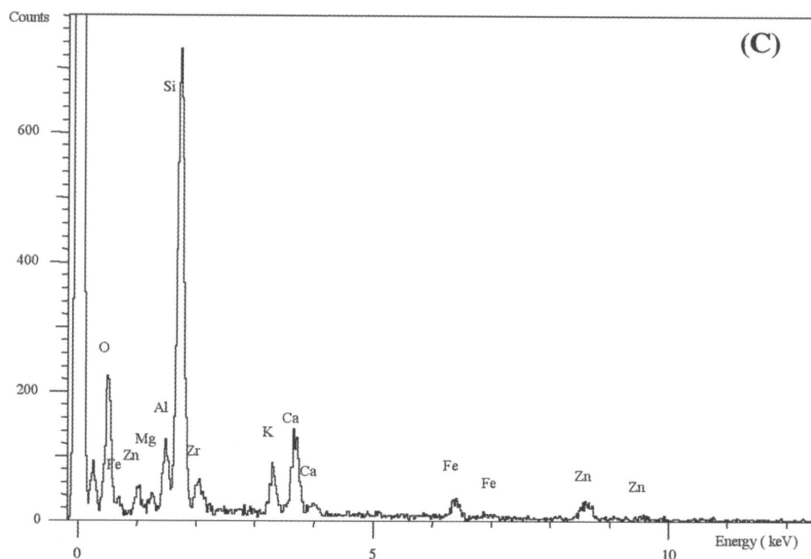


Figure 2. (C): Overall EDX spectrum of the optical field (B) in which the presence of Fe is detected. Results obtained with samples with 0.6% cation content, heat treated at 820°C for 5 min.

The roughness of the films, measured by the conventional method of a sliding pick-up, is similar in all of these on a millimetric scale (the pick-up slides 5 to 6 cm in order to average the roughness), with values of  $R_a=0.05 \mu\text{m}$ . On a more local level, using the differential interferometry technique (Figure 3) with which analyses of a micrometric order are performed (the analyzed field is  $0.1 \times 0.1 \text{ mm}$ ), greater roughness is observed in the deposited films (Ti,  $R_a=21\text{nm}$ ; Fe,  $R_a=40\text{nm}$  and Co,  $R_a=34 \text{ nm}$ ) than in the glaze ( $R_a=18 \text{ nm}$ ). This greater local roughness is explained when the deposited films are examined by atomic force microscopy (AFM), by which nanometric levels are reached. In effect, as Figure 4 shows, in every case there are nanocrystal aggregates. The size of these microaggregates is smaller in the case of titanium, whose mean diameter is around  $\phi=50 \text{ nm}$ , whereas in the case of cobalt and iron these are larger, reaching diameters around  $\phi=75\text{nm}$ . The inference can be made that in spite of a difference in local roughness, since the roughness on a millimetric scale of the deposited films is equal to that of the glaze, the gloss development effect stems fundamentally from the greater reflectivity of the crystallized oxides.

The UV-V-NIR spectra of the iron, cobalt and titanium films are shown in Figure 5, compared respectively with the corresponding spectra of hematite, cobalt spinel and anatase. The iron film spectrum is similar to that of hematite with bands assignable to Fe(III) in octahedral coordination. The cobalt film spectrum indicates the presence of cobalt (III) in octahedral coordination with the bands associated with  $^1A_{1g} \rightarrow ^3T_1$  (1200 nm, spin-forbidden band),  $^1A_{1g} \rightarrow ^1T_1$  (700 nm) and  $^1A_{1g} \rightarrow ^1T_2$  (285 nm). Furthermore, the band between 450-500 nm can be associated with Co(II) in tetrahedral coordination (transition  $^4A_{2g}(F) \rightarrow ^4T_1(P)$ ). Finally, the titanium film spectrum only displays the ligand-metal charge transfer doublet at 220 and 330 nm<sup>[10]</sup>. In every case, when comparing the oxide precipitate film spectrum with that of the powdered oxide, a shift of the bands to lower wavelengths can be observed due to quantum effects related to the nanometric size of the particles. When applying the elementary model of the electron-hole pair in a potential well, usually employed to explain the optical properties of small colloidal particles and thin films (Eq. 5), the radius can be estimated of the nanocrystals that make up the aggregates of the film at 5.2 nm for iron, 11.3 nm for cobalt and 14 nm for titanium.

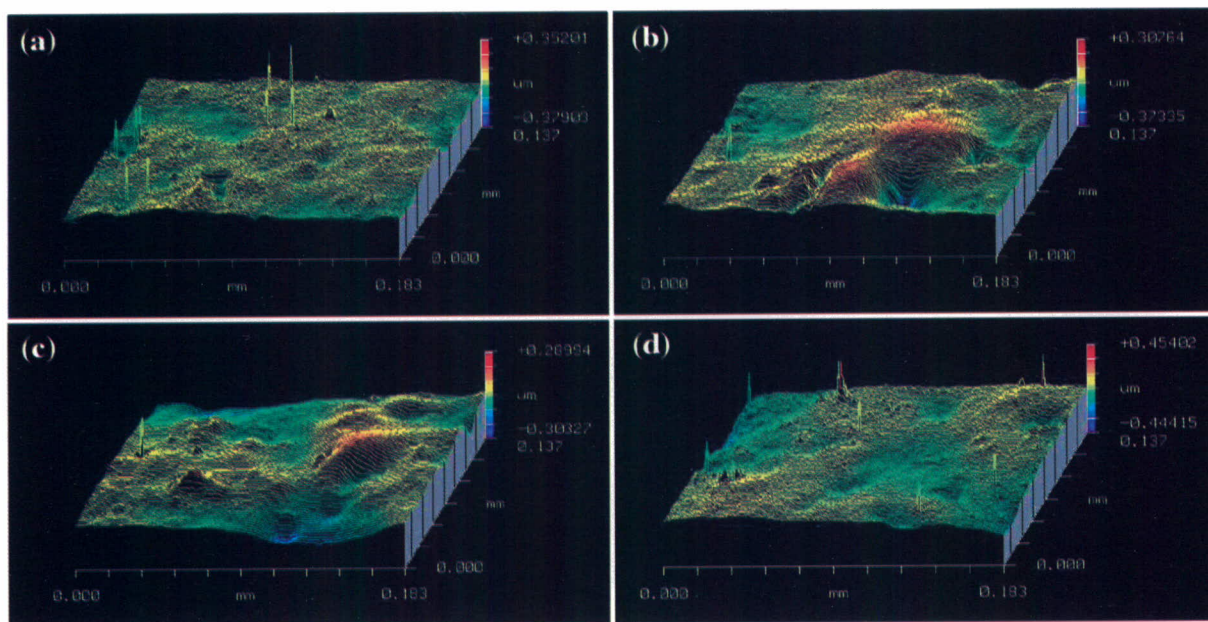


Figure 3: Differential interferometry topography of the base glaze and films with 0.6% cation, heat treated at 820°C for 5 min. (a) Base glaze. (b) Hematite film. (c) Co<sub>3</sub>O<sub>4</sub> film. (d) Anatase film.

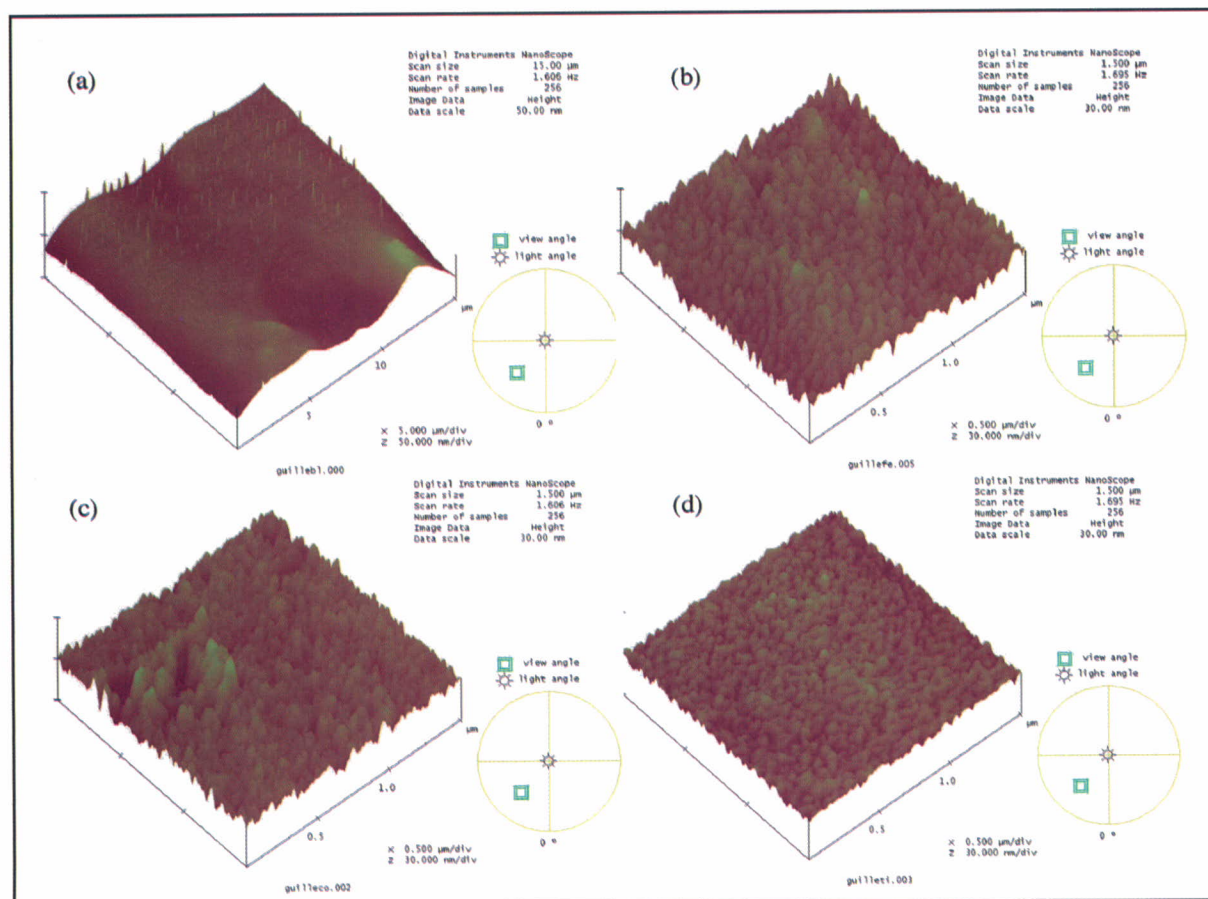


Figure 4: AFM images of the base glaze and films with 0.6% cation, heat treated at 820°C for 5 min. (a) Base glaze. (b) Hematite film (aggregate size  $\phi = 75$  nm). (c) Co<sub>3</sub>O<sub>4</sub> film ( $\phi = 75$  nm). (d) Anatase film ( $\phi = 40$  nm).

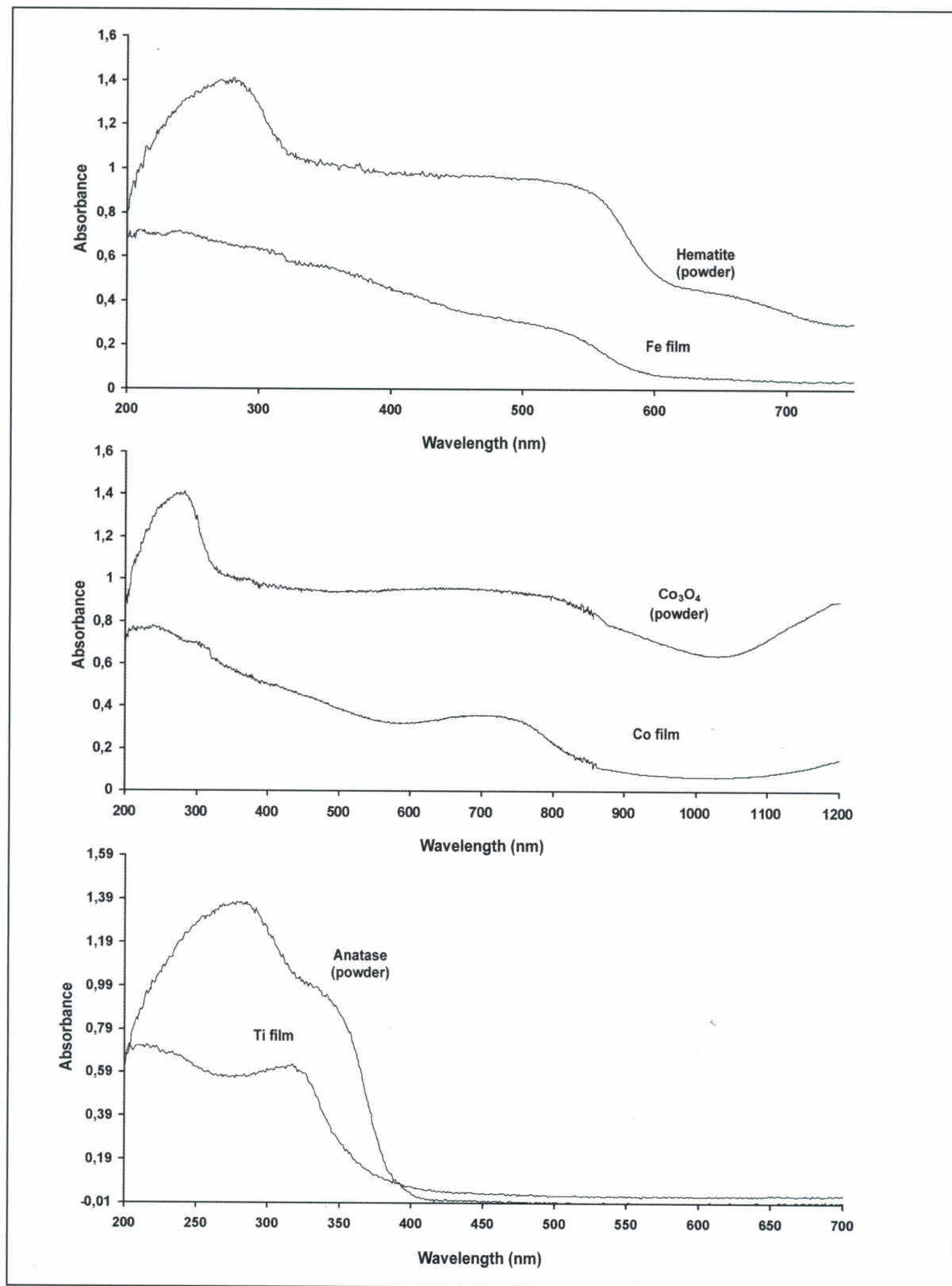


Figure 5: Espectroscopía UV-V-NIR de las películas con 0.6% del catión y tratadas a 820 °C durante 5 minutos comparadas con polvo de hematita,  $\text{Co}_3\text{O}_4$  y anatasa.

The results discussed above are consistent with the layer formation model described in section 3.1: heterogeneous nucleation of oxides from the inks lead to the formation of a great number of nanocrystals that form individualized clusters or aggregates, also of nanometric size, which grow parallel to each other and normal to the surface.

### 3.3. EFFECT OF METAL CONCENTRATION ON THE MICROSTRUCTURE OF ANATASE FILMS

As the lustre effect develops with remarkable intensity in the anatase films, the results obtained on applying inks containing increasing concentrations of titanium, prepared by the method described previously, are discussed below. All the samples were subjected to heat treatment at a peak temperature of 820°C and 5-min residence time at this temperature.

Figure 6 depicts the evolution of the UV-V-NIR spectra of these samples compared with the spectrum of powdered anatase. The spectra of the deposited films are observed to exhibit the semiconductor charge transfer doublet at lower wavelengths than the case of the powdered anatase. As previously set out, these spectra enable estimating the radius of the anatase nanocrystals that make up the film. This estimation is made by measuring the absorption threshold wavelength on the spectra, then calculating the semiconductor band gap energy from this and applying the equation of quantum confinement in a potential well of the electron-hole pair (Eq. 5). The results obtained as a function of the titanium concentration in the sample are shown in Figure 7, in which a relative minimum nanocrystal size (radius 13.1 nm) can be observed around a 1.1% titanium concentration in the ink.

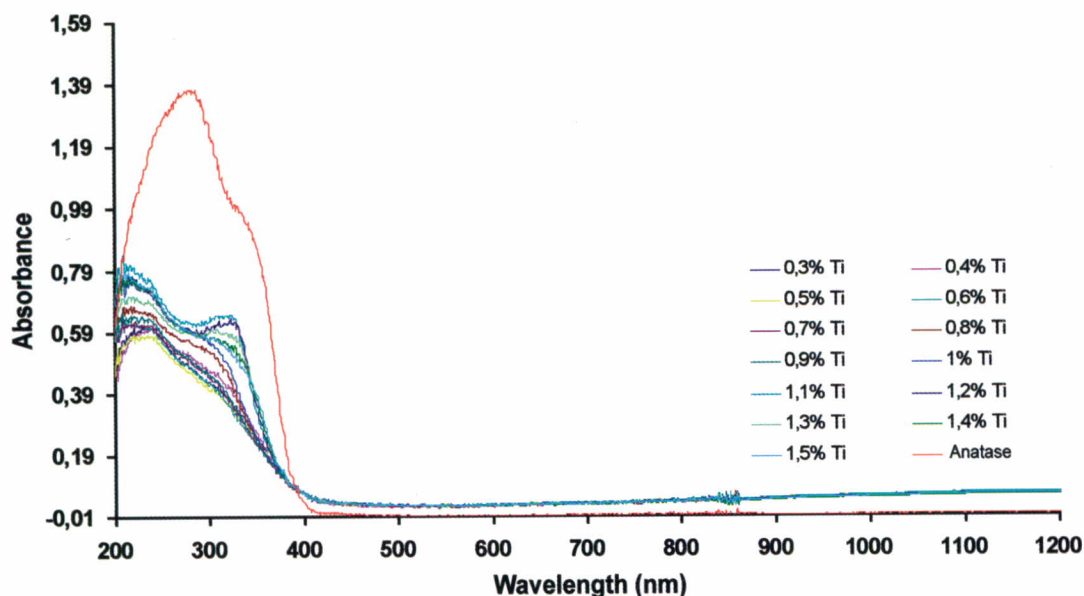


Figure 6. Evolution with Ti concentration of the UV-V-NIR spectra of the films heat treated at 820°C for 5 min.

The evolution of the gloss measurements (Figure 7) also indicates the existence of a relative maximum gloss around 1.1% titanium in the ink, this relative maximum gloss zone being associated with the minimum values of the size of the nanocrystals making up the film. As the crystals begin to grow and there is a greater saturation of crystals at the surface, gloss decreases.

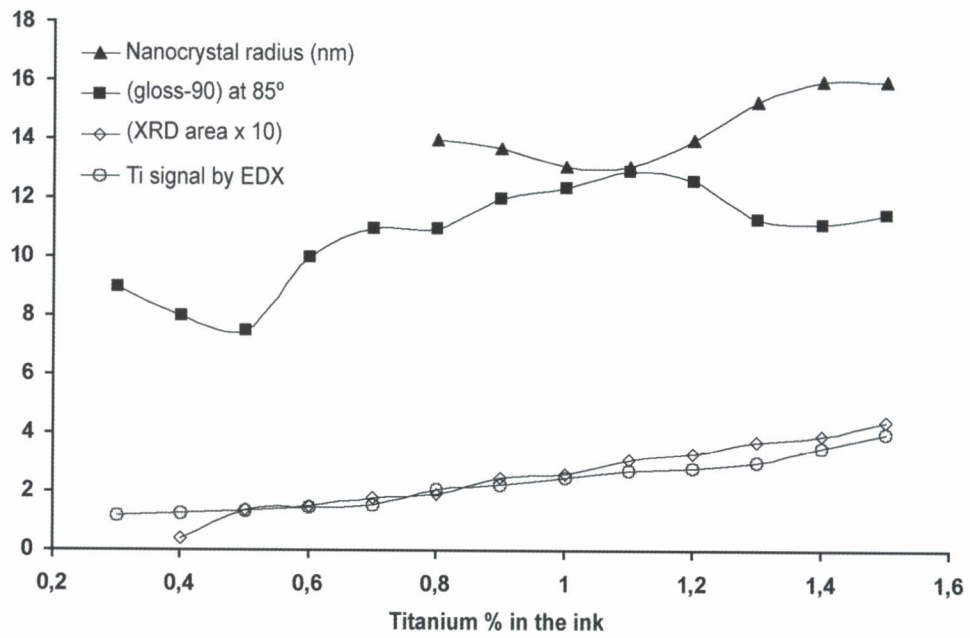


Figure 7. Variation of nanocrystal size, film gloss, anatase peak area and Ti signal by EDX, expressed as %TiO<sub>2</sub>, as a function of titanium content in the ink.

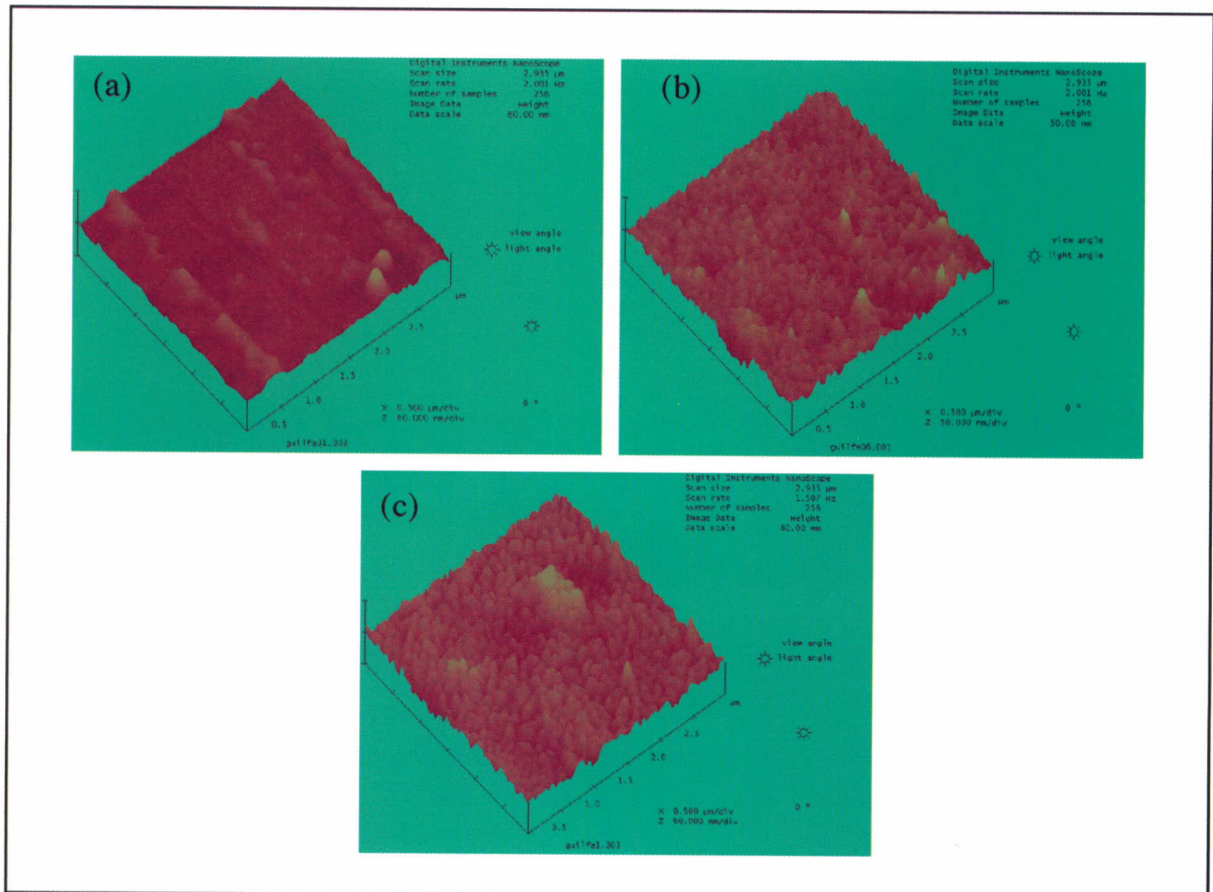


Figure 8. AFM images of films with different Ti concentrations and local roughness data measured by interferometry: (a) 0.3 % Ti.  $R_a = 44 \text{ nm}$  (b) 1% Ti.  $R_a = 33 \text{ nm}$  (c) 1.5 % Ti.  $R_a = 51 \text{ nm}$ .

Together with nanocrystal radius and film gloss, Figure 7 also plots the values of the anatase diffraction peak area ( $2\theta = 25^\circ$ ) and the signal obtained for titanium by X-ray energy dispersion analysis expressed as %TiO<sub>2</sub>. Both signals can be observed to grow analogously when the titanium content in the sample is increased, which indicates that practically all the added titanium crystallizes in the form of anatase, enriching the film with nanocrystals.

The evolution of film local topography with concentration monitored by AFM, and the local roughness measured by differential interferometry, are shown in Figure 8. It can be observed that at low ink concentrations, the covering power is inadequate and crystallized regions appear next to virgin regions, while roughness is relatively high. When the concentration is increased, all the areas are uniformly covered and agglomerates appear that have grown normal to the surface, producing a slightly lower roughness. Finally, at high titanium concentrations in the ink, some of the agglomerates are observed to grow, generating less uniform crystallization and raising roughness again.

### 3.4. EFFECT OF TEMPERATURE ON ANATASE FILM MICROSTRUCTURE

Figure 9 depicts the evolution of the UV-V-NIR spectra of the films based on heat-treatment temperature (from 820 to 1025°C), in each case with a residence time of 5 minutes and 0.6% titanium concentration. Nanocrystal size was again calculated from these spectra; these results are plotted in Figure 10 with the evolution of gloss and the anatase diffraction peak area ( $2\theta = 25^\circ$ ).

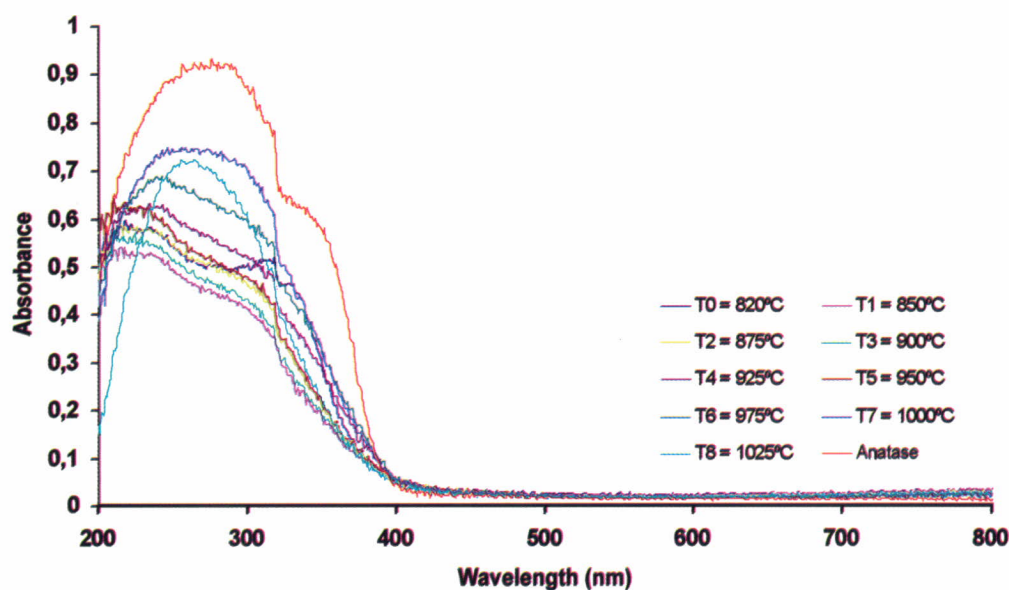


Figure 9. Evolution with temperature of the UV-V-NIR spectra of films with 0.6% Ti content in the ink.

Nanocrystal size is observed to increase from 13.5 nm at 820°C to a stable maximum size (estimated at 35.8 nm) above 950°C. In contrast, gloss decreases as temperature increases until reaching a similar value to that of the glaze. An analogous evolution is found in the value of the diffraction peak area: at the peak temperature tested (1025°C) the presence of anatase is thus practically not detected. These results are in agreement with the proposed film-glaze interaction model, so that at

temperatures approaching glaze softening (established at 1040°C), the film disappears owing to the combined effect of solubilization-volatilization.

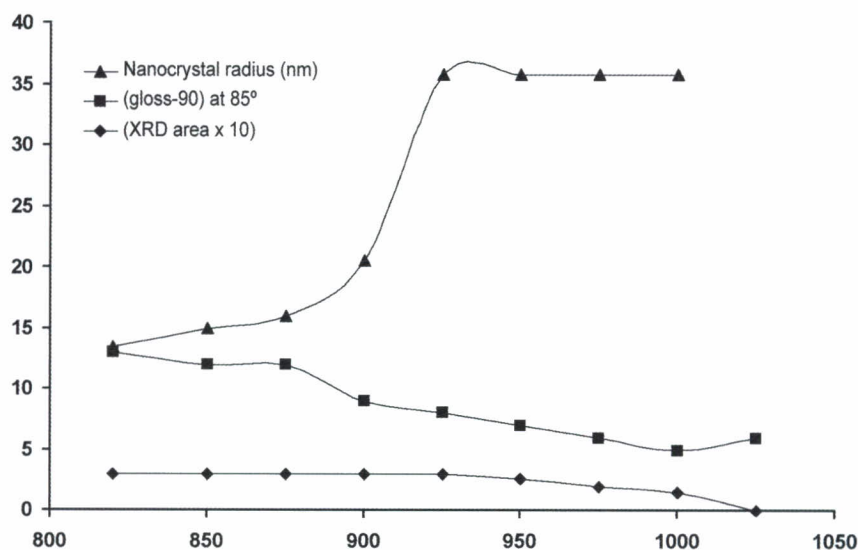


Figure 10. Variation of nanocrystal size, film gloss and anatase peak area as a function of heat-treatment temperature. 0.6% Ti content in the ink.

### 3.5. EFFECT OF RESIDENCE TIME AT MAXIMUM TEMPERATURE.

Figure 11 shows the evolution of the UV-V-NIR spectra of the films obtained using an ink with 1% titanium content, at a heat-treatment temperature of 925°C and different residence times. Once again, the threshold wavelength is observed to be lower for the film spectra than for the powdered anatase. On the other hand, although the intensity of the bands descends slightly with heat-treatment time, the semiconductor band gap energy is the same; the radius of the nanometre particles therefore remains constant, and is estimated at 18.3 nm by means of Eq. 5.

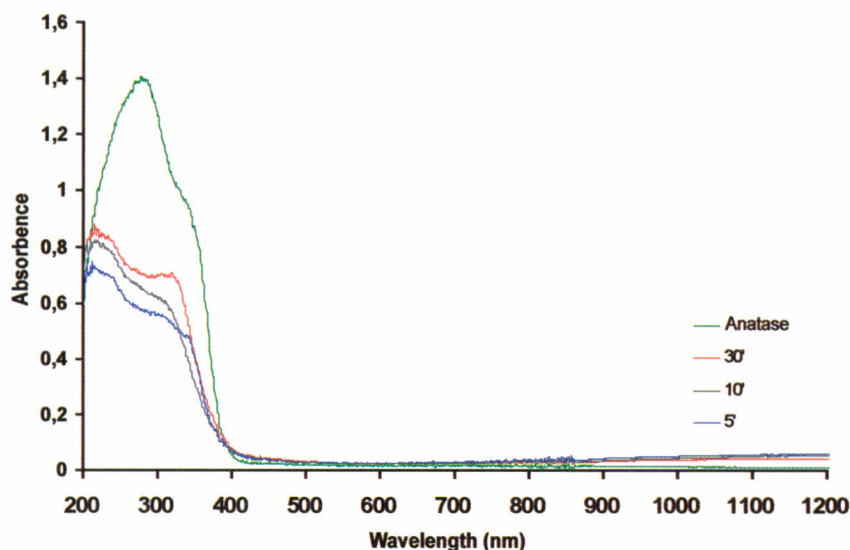


Figure 11. Evolution with heat-treatment time of the UV-V-NIR spectra of films with 1% Ti content in the ink heat treated at 925°C.

Table 2 details the results of gloss and anatase diffraction peak area ( $2\theta=25^\circ$ ) at the heat-treatment temperatures of 925 or 820°C at different residence times. At 925°C, which is higher than glaze sintering temperature, anatase concentration and gloss decrease as heat-treatment time increases, owing to titanium solubilization in the glaze. In contrast, at 820°C there is no significant loss of anatase with residence time and gloss remains steady, as was to be expected at a temperature where the glaze maintains a very high viscosity.

Heat treatment temperature (°C)	Residence time (min.)	Gloss at 85 °	XRD area (counts x degree)
820	0	100.5	28
	5	101.9	30
	10	100.8	32
	20	101.4	30
	30	98.0	32
925	0	100.1	32
	5	91.4	30
	10	85.2	26
	20	80.2	25
	30	77.5	25

Table 2: Values of gloss and diffraction peak area of anatase in films with 1% Ti in the ink at different heat-treatment temperatures and residence times.

#### 4. CONCLUSIONS.

The foregoing study enables drawing the following conclusions:

1. The formation of high reflectivity films by screen printing application of inks that contain dissolved iron nitrate (III) nonahydrate, cobalt nitrate (II) hexahydrate or t-butoxide, on a conventional previously fired glaze, with subsequent heat treatment at a temperature higher than 800°C, is due to the crystallization of a fine layer of hematite, cobalt spinel and anatase respectively, as shown by grazing incidence X-ray diffraction.

2. The films developed display a macroscopic roughness similar to that of the original glaze, so that the greater reflectivity of these films stems from the presence of crystals with a high refractive index. Of the studied cases, the most significant one has been that of the anatase film. With a refractive index of 2.6, this film yields a gloss of 103, as opposed to the base glaze that has a gloss of 96 and a refractive index of 1.6-1.7.

3. The films are made up of crystalline aggregates that have grown from the surface of the glaze in a process of heterogeneous nucleation. These aggregates, in turn, consist of nanocrystals, whose radius, estimated by the method of quantum confinement in a potential well of the semiconductor electron-hole pair, in films heat treated at 820°C for 5 minutes, was 5.2 nm for hematite, 11.3 nm for the cobalt spinel and 14.0 nm for anatase.

4. When the titanium concentration in the ink is varied, the deposited films exhibit a minimum crystal radius associated with a relative maximum gloss. Local roughness is relatively high for titanium concentrations in the ink below 0.5%, which

is associated with the presence of non-crystallized zones in the surface. When the concentration is increased, the surface becomes uniformly covered with crystals, causing roughness to decrease and gloss to rise. However, at concentrations exceeding 1.3% titanium, some aggregates grow more than others, increasing roughness and reducing gloss.

5. The gloss of Ti films and the presence of anatase crystals in these films decrease as heat-treatment temperature rises, until these crystals almost completely disappear at a temperature of 1025°C, close to the glaze softening temperature, determined by hot stage microscopy. This behaviour is due to the combined effect of volatilization and solubilization of the crystals in the partially softened glaze. Crystal size initially grows with temperature (coarsening), to stabilize at sizes estimated at 35.8 nm, probably already larger than the Bohr radius for anatase.

6. The effect of heat-treatment time depends on whether the temperature is lower or higher than glaze sintering temperature. In the former case, the Ti film is quite steady, without any significant variation in gloss or presence of anatase crystals. However, if the heat-treatment temperature exceeds glaze sintering temperature, the lower glaze viscosity destabilizes the film, reducing both gloss and the presence of anatase crystals. With regard to crystal size, this is observed to remain constant, independently of heat-treatment time, with an estimated crystal size of 18.3 nm at 925°C.

7. The analyzed behaviour follows a simple model of heterogeneous nanocrystal crystallization with growth in aggregates in the direction normal to the surface and parallel to each other, from the carbonized amorphous material in fusion on the glaze. Subsequently, glaze viscosity, solubility of the oxide in the glaze and volatility of the oxide in the film, determine the destabilization and later loss of the film, depending on the applied thermal treatment.

## REFERENCES.

- [1] C.S. HURLBUT, C. KLEIN, *Manual de Mineralogía de Dana*, Reverté, 1989.
- [2] RICHERSON, D.W.: *Modern Ceramic Engineering*, 2<sup>nd</sup> Ed., Marcel Dekker, New York, 1992
- [3] F. LAMILLA, E. WAGG, *Decoration Techniques for Single-Fire, Fast-Fire Tile Production*, *Ceram. Eng. Sci. Proc.*, 16 (1995) 80-81.
- [4] R.P. GOEHNER, M.O. EATOUGH, A study of grazing incidence configurations and their effect on X-ray diffraction data, *Powder Diffraction* 7(1992)2-5.
- [5] AL. L. EFROS AND A.L. EFROS, *Interband Light Absorption in Semiconductor Spheres*, *Sov. Phys. Semicond.*, 16(1982)772-77.
- [6] S. FIUGGE, in *Practical quantum mechanics*, ed. Springer, Berlin, Vol. 1, 1971.
- [7] CIE Comission International de l'Eclairage, *Recommendations on uniform color Space, Color Difference equations, Physhometrics Color Terms, Supplement n°2 de CIE*, Pub. N°15(E1-1.31)1971, Bureau central de la CIE, Paris (1978).
- [8] J.E. SHELBY, *Introduction to Glass Science and Technology*, RCS Paperbacks eds., 1997.
- [9] P.W. MCMILLAN, *Glass-Ceramics*, Academic Press, 2a. ed., New York 1979.
- [10] A.B.P. LEVER, *Inorganic Electronic Spectroscopy*, 3<sup>rd</sup> ed, Elsevier, Amsterdam, 1997.